PULSATION AND MASS LOSS IN MIRA VARIABLES

P. R. Wood
Mount Stromlo and Siding Spring Observatory
Research School of Physical Sciences,
Australian National University

Abstract

The behaviour of pulsation in the outer layers of a "typical" Mira variable ($M = M_\odot$, $L = 10^4 L_\odot$, $T_{eff} = 2750K$, $P = 373$ days) has been studied in the adiabatic and isothermal limits. A shock wave propagates outward once per period and the radial velocity obtained from observations of hydrogen emission lines is identified with the velocity of gas in the post-shock region. In the adiabatic case, mass loss in the form of a steady stellar wind was produced. However, the mass loss rate is far too large (0.02 $M_\odot yr^{-1}$) if approximate observational estimates of the photospheric density are adopted. In the isothermal case, no continuous mass loss was produced but occasional ejection of shells occurs. The time-averaged mass loss rate produced by this process is $\approx 10^{-12} M_\odot yr^{-1}$. Pulsation introduced into a star undergoing steady mass loss as a result of radiation pressure acting on grains caused the mass loss rate to increase by a factor of ~ 40 while the terminal velocity of the flow was almost unaltered.

I. INTRODUCTION

The occurrence of violet displaced resonance line absorption in the spectra of luminous M giants and supergiants has long been interpreted as evidence for the existence of matter flowing outward from these stars at ~ 10 km sec^{-1} (Deutsch 1960, Weyman 1963), although the mass loss rates are still very uncertain (Sanner 1976, Reimers 1977, Bernat 1977). In addition, infra-red (IR) observations have shown the existence of a cool emission component in many M giants and supergiants which is taken to indicate the presence of dusty circumstellar material. Mass loss rates have been derived from the IR observations by Gehrz and Woolf (1971). The production of mass outflow in late-type stars is usually attributed to a radiation pressure force acting on grains (Hoyle and Wickramasinghe 1962, Kwok 1975) or possibly on molecules (Weyman 1962, Maciel 1977), or to chromospheric heating produced by sound generation in the extensive convection zones of these stars (Fussi-Pecci and Renzini 1976, Renzini et al. 1977). However, in the case of the Mira variables, a large amplitude shock wave is injected into the outer layers of the star once each pulsation cycle so that mass loss may be produced by pulsation alone, or the pulsation may substantially increase the rate of mass loss which results from either of the above mechanisms. In this paper, the production of mass loss by pulsation and the effect of pulsation on mass flows produced by radiation pressure acting on grains are examined.

II. OBSERVATIONAL DATA

It will be assumed here that the variability of Miras is the result of a radial pulsation which causes a shock to propogate into the outer layers of the star once each pulsation cycle. The bright hydrogen emission lines that are apparent during much of a Mira pulsation cycle are assumed to originate from the relaxation region behind the outward propagating shock wave. In this situation, the velocity of the hydrogen emission lines represents the velocity of the material behind the shock front. Similarly, the velocity of the violet-shifted cores of strong resonance absorption lines is taken as a measure of the velocity of a steady stellar wind far above the shocked region near the photosphere.

The existence of a characteristic double-peaked maser emission from a number of Mira variables provides an accurate means of determining centre-of-mass (cms) radial velocities for these stars. According to the maser models of Elitzer, Goldreich and Scoville (1976) and Reid et al. (1977), the double-peaked structure results from maser amplification on the near and far sides of a spherically symmetric flow of matter from the central star. The velocity separation of the two peaks, which is observed to be time invariant (Harvey et al. 1974), is assumed to be twice the terminal flow velocity. A comparison of maser and thermal radio emission velocities (Reid and Dickinson 1976) confirms the prediction that the mean of the radial velocities of the two maser emission peaks coincides with the cms radial velocity of the associated star.

Table 1 lists cms radial velocities derived for all Mira variables for which either thermal radio emission or well-defined twin maser emission peaks could be found in the literature. Also listed are hydrogen emission line velocities and absorption line velocities (Feast 1963, Wallerstein 1975) relative to the cms of the star (a positive entry indicates motion outward from the star): these velocities are obtained at, or shortly after, maximum. No correction factor (usually 24/17) has been applied to the emission line velocities to account for sphericity and limb darkening effects. In fact, for an optically thick shock or an optically thin shock with overlying absorption, the peak emission line intensity should occur at the shock velocity and therefore no correction factor should be applied in these cases. Column 8 of Table 1 gives the estimate of the terminal stellar wind velocity obtained from resonance line absorption (Wallerstein 1975) while column 9 gives the terminal velocity estimate which is equal to half the velocity separation of the twin OH maser emission peaks.

The velocities given in Table 1 are plotted against the period of pulsation in Figures 1 and 2. In most stars, the post-shock velocity lies in the range 5 to 10 km s^{-1} near maximum light, with some evidence for an increase in the outward velocity with period. Absorption line velocities lie in the range -5 to -10 km s^{-1}, but these velocities are of little use in the present situation since a lack of knowledge of their region of formation in the shocked atmosphere precludes any comparison of these velocities with theoretical models. The terminal flow velocities (Fig. 2) obtained from circumstellar absorption lines and from the separation of the twin maser emission peaks seem to agree reasonably well and they are concentrated in the range 3-6 km s^{-1}. There is an apparent increase in the terminal flow velocity with period which is generally consistent with the relation obtained from the larger sample of stars which includes the semi-regular variables with periods $\gtrsim$ 500 days (Dickinson, Kollberg and Yngvesson 1975).

Table 1

MIRA RADIAL VELOCITIES

Star	Period	v_{cms}	v^W_{abs}	v^F_{abs}	v^W_{em}	v^F_{em}	v_{cs}	$\frac{1}{2}\Delta v_{OH}$	Source
Z Cyg	263	-171.0				2.0		2.2	1
R Aql	284	30.1	-5.4	- 3.9	5.1	9.1	7.1	6	2
R Leo	313	7.2	-7.8	- 4.8	7.2	9.2	0.7		3
O Ceti	332	50.9		-13.9		2.9			4
U Mic	335	- 63.0		- 9.0		5.0		3	5
RS Vir	353	- 25.0				15.0		3.5	1
SY Aql	356	- 71.1				11.9		3.5	1
S Cr B	360	- 15.6	-6.3	-14.6	5.9	6.4		3.5	1
U Ori	372	- 26.0	-6.0	- 4.0	6.0	8.0	3.0	3.5	10
V Mic	381	- 0.1						5.6	6
W Hya	382	37.7	-7.3	- 4.3	~1.7	9.3	4.2	4	7,3,8
R Hya	388	- 12.3	-5.8	- 6.3	6.7	6.7	11.2		11
RW Sco	388	- 78.8				9.2		5	5
W Vel	393	4.0		- 4.0		8.0		3.5	5
RR Aql	394	12.6				11.6		5	2
U Her	406	- 33.0	-6.0	- 5.0	6.0	11.0		5	10
χ Cyg	407	- 8.9	-8.9	- 8.9	7.1	7.1	7.6		4
WX Ser	425	- 10.5						7.5	2
R Cas	431	16.6	-6.4	- 9.4	8.1	6.6	3.6	3.5	3,9
W Aql	490	- 39.6				- 1.6			11
IK Tau	~500	46.3					~9.7	17	2

Notes: Period is in days and velocities are in km s^{-1}. v_{cms} is the heliocentric radial velocity of the star and all other velocities are measured relative to this value. v^W_{abs} and v^F_{abs} (v^W_{em} and v^F_{em}) are absorption (emission) line velocities measured near maximum by Wallerstein (1975) and Feast (1963) respectively. v_{cs} are circumstellar absorption line velocities from Wallerstein (1975) and $\frac{1}{2}\Delta v_{OH}$ is half the velocity separation of the twin OH maser emission features. Sources of v_{cms} are: (1) Dickinson, Kollberg and Yngvesson (1975); (2) Wilson and Barrett (1972); (3) Reid and Dickinson (1976); (4) Lo and Bechis (1977); (5) Bowers and Kerr (1977); (6) Caswell, Robinson and Dickel (1971); (7) Dickinson and Kleinmann (1977); (8) McGee, Newton and Brooks (1977); (9) Nguyen-Quang-Rieu, Fillet and Gheudin (1971); (10) Wilson et al. (1972); (11) Dickinson et al. (1978).

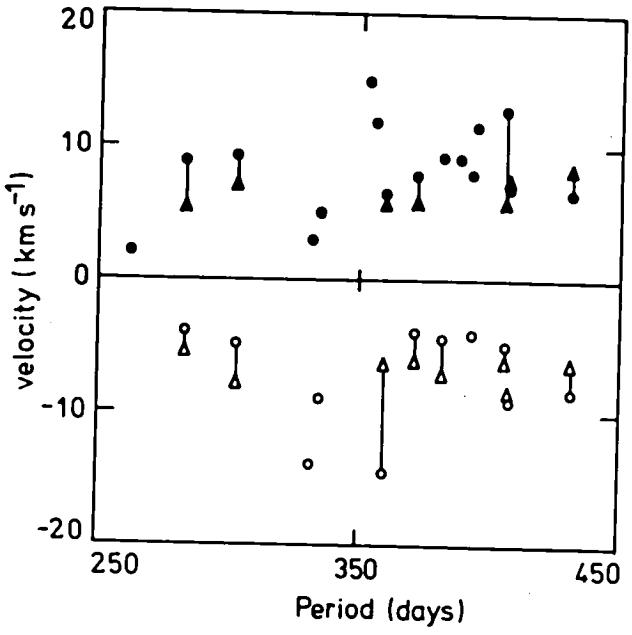

Fig. 1 Emission line (solid symbols) and absorption line (hollow symbols) velocities near maximum plotted against period. Circles are from Feast (1963) and triangles from Wallerstein (1975). Lines join measurements of the same star by the two different authors. All velocities are measured relative to the centre-of-mass of the star.

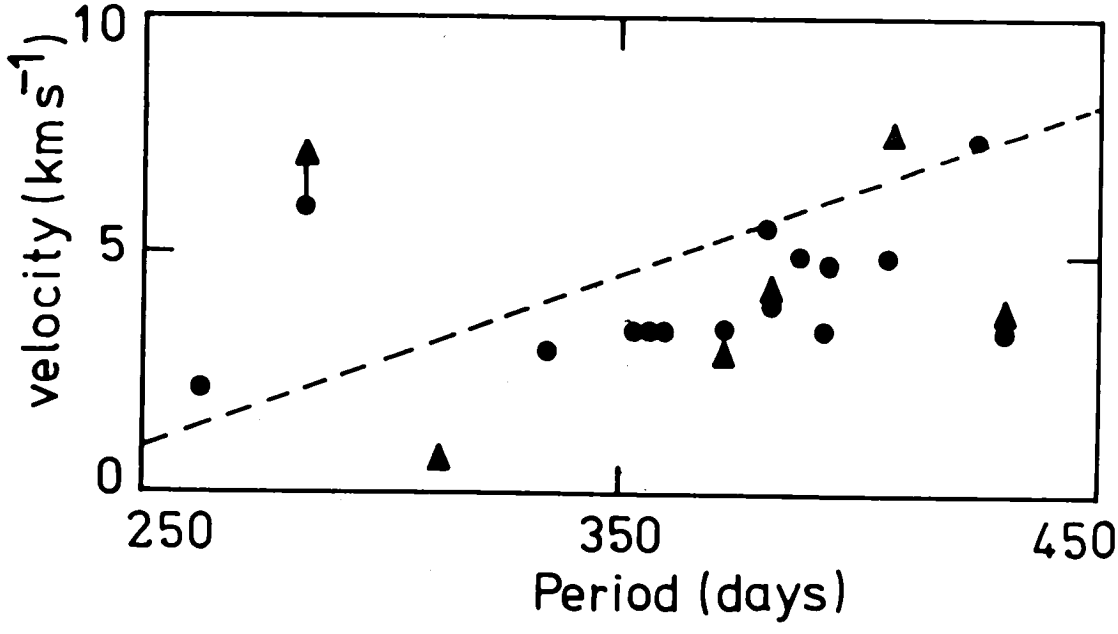

Fig. 2 Stellar wind flow velocity obtained from circumstellar optical absorption lines (triangles) and half the velocity separation of twin OH maser emission peaks (circles) plotted against Mira period. Lines join observations of the same star. The dotted line is the relation obtained by Dickinson, Kollberg and Yngvesson (1975) for a larger sample of stars including semi-regular variables with periods > 500 days.

The most useful observational property for comparison with theoretical models is the variation in the hydrogen emission line (i.e., post-shock) velocity with phase. However, the existing emission line velocity curves seem rather ambiguous. Early velocity curves obtained at dispersions of 35-65 A mm^{-1} for O Ceti (Joy 1926) and U Ori, R Leo, χ Cygni and R Cas (Merrill and Burwell 1930) are shown in Figure 3a after conversion to velocity relative to the stellar centre-of-mass. These curves generally show a rise to maximum at phase ~ 0.2 and decline thereafter. However, more recent higher dispersion results (~ 10 A mm^{-1}) by Joy 1954, Merrill 1945, 1945a, 1947, 1952, 1953 and Wallerstein 1975 (Fig. 3b) do not show any consistent pattern, e.g., R Leo and O Ceti show a maximum velocity at phase ~ 0.2 as found in earlier results whereas R Hya shows a continually increasing velocity and χ Cygni and U Ori show a continually decreasing velocity. In view of the discrepancy between the two sets of results, perhaps all that one can say from the observations is that the velocities of the hydrogen emission lines lie in the range 5-10 km s^{-1}.

III. NUMERICAL METHODS AND PHYSICAL ASSUMPTIONS

This study uses an implicit difference scheme based on the Eulerian fluid dynamical equations expressed in conservation law form. The calculations were performed on a model with parameters $L = 10^4 L_\odot$, $M = M_\odot$ and composition (X,Y) = (0.7, 0.3). These parameters were chosen since the Mira pulsation period (373 days) obtained for the star from the formulae of Wood and Cahn (1977) lies near the centre of the observed period distribution (Wood and Cahn 1977). A period of 373 days is also representative of the periods of those Miras which are observed to have maser emission.

For the hydrostatic starting models, an effective temperature T_{eff} = 2750K is derived by assigning the star to the old disk giant branch (Wood and Cahn 1977) and a photospheric radium r_{phot} is defined by the relation $L = 4\pi r_{phot}^2 T_{eff}^4$. The radial temperature distribution in the starting models (and at all times in the isothermal model sequences) is given by

$$T = \tfrac{1}{2} T_{eff} \left(1 + \tfrac{3}{2} \tau\right) f \qquad (1)$$

where $f = 1$, if $r < r_{phot}$,

$$= 1 - \left(1 - \frac{r_{phot}^2}{r^2}\right)^{\frac{1}{2}} \quad , \text{if } r > r_{phot}.$$

The factor f accounts for geometric dilution of radiation at large distances from the photosphere. A fictitious optical depth τ is defined as an explicit function of r by

$$\tau = \tfrac{2}{3} \exp\left\{-\frac{(r - r_{phot})}{\lambda}\right\}$$

where the scale height λ is chosen so that $T = 10^4$K on the inner boundary which is situated at $r = 0.8\ r_{phot}$. The inner boundary conditions were applied at $0.8\ r_{phot}$ since Mira variables appear to be first overtone pulsators (Wood 1975) and first overtone pulsation models have a node near $0.8\ r_{phot}$. Stellar interior models constructed using radiative diffusion and mixing-length convection for energy transport indicate that the temperature at $0.8\ r_{phot}$ is ~ 10^4K, although this is dependent on the molecular opacity

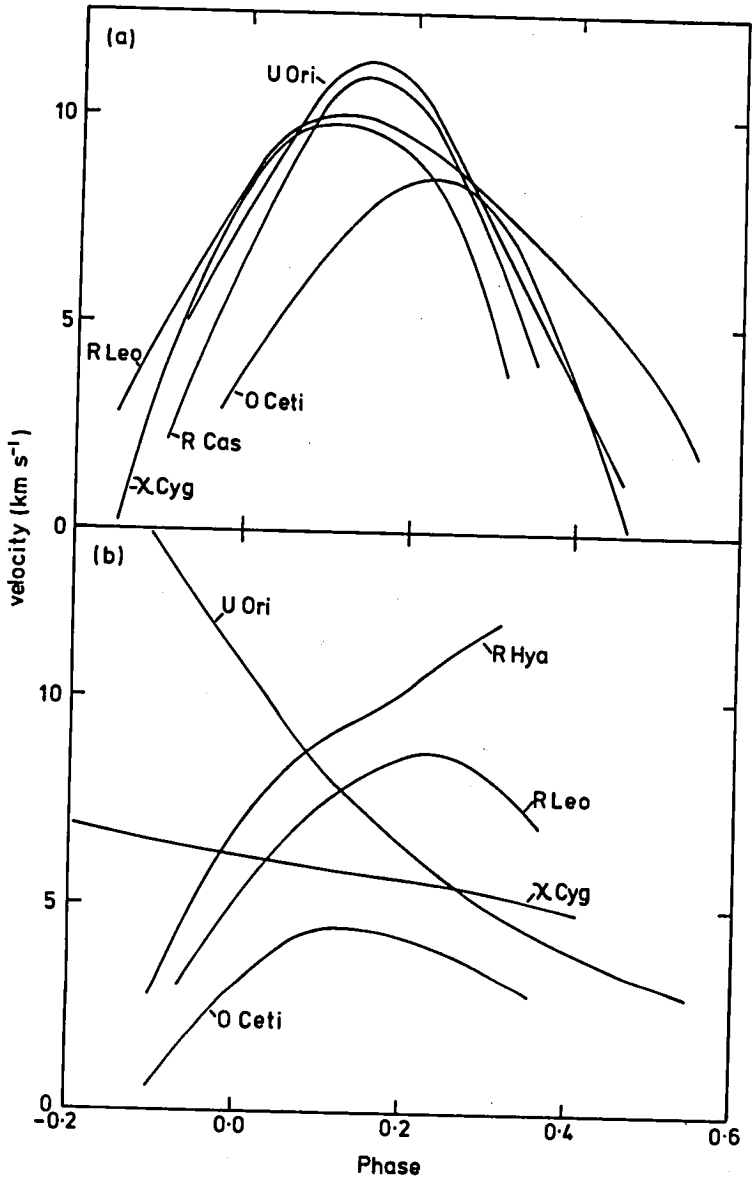

Fig. 3a Emission line velocity relative to the stellar centre-of-mass plotted against phase of the pulsation cycle. The curves are eye-fits to the data of Merrill and Burwell (1930) and Joy (1926).

Fig. 3b Same as Figure 3a except data are from Merrill 1945, 1945a, 1947, 1952, 1953 and Wallerstein (1975).

assumed in the photospheric layers.

In the hydrostatic models, the pressure Π_o applied at the inner boundary was adjusted so that, at fictitious optical depth $\tau = \frac{2}{3}$, the gas pressure $P_g = 10^2$ dynes cm^{-2}($\rho \approx 6 \times 10^{-10}$ gm cm^{-3}) to agree with observational and model atmosphere estimates of the photospheric density in late type giants and Miras (Auman 1969, Fujita 1970). Pulsation of the star is simulated by varying the pressure Π applied at the inner boundary according to the formula

$$\ln\Pi = \ln\Pi_o + A \sin \frac{2\pi t}{P} \quad , \tag{2}$$

where P is the Mira pulsation period (373 days).

In models where an approximate simulation of a mass flow produced by radiation pressure acting on grains is required, it is assumed that the gas and grains are coupled and that all grains condense out over a small temperature interval. In this situation, the radiation force per unit mass of gas is approximated by

$$f_{rad} = \frac{Q_{eff}}{1 + \exp \frac{T - T_{con}}{\Delta T}} \frac{L}{R^2} \tag{3}$$

where Q_{eff} is a constant, T_{con} is a condensation temperature and ΔT is a temperature interval over which all material condenses out. The values T_{con} = 1500K and ΔT = 100 K are used here.

The equation of state allows for the formation of molecular hydrogen but ionization of hydrogen and helium (applicable only in the innermost zones) had to be omitted because of numerical problems at the inner boundary.

In all calculations, the outer boundary was placed at $10r_{phot}$ and zone spacing δr increased with r according to the formula $\delta r \propto r^{\frac{1}{2}}$. The radius r and the Eulerian coordinate x are related by the formula

$$r = 8.88 \times 10^7 \ (501 - x)^{-2} \ (R_\odot) \ .$$

For the adiabatic and isothermal calculations not involving radiation pressure 360 zones were used while 180 zones were used in the calculations involving radiation pressure induced flows.

IV. ADIABATIC MODELS

Using an amplitude A = 1 in equation 2, a sequence of adiabatic models was constructed covering 17 pulsation periods, by which time a steady periodic situation had been reached. Figure 4 shows the propagation of the first 10 shocks from the inner to the outer boundary as a function of time while Figure 5 shows the radial density, temperature and velocity distributions at one value of the phase of the pulsation cycle in the steady periodic limit.

In Figure 4, it is noticeable that the first shock which propagates into the hydrostatic atmosphere travels much faster than succeeding shocks.

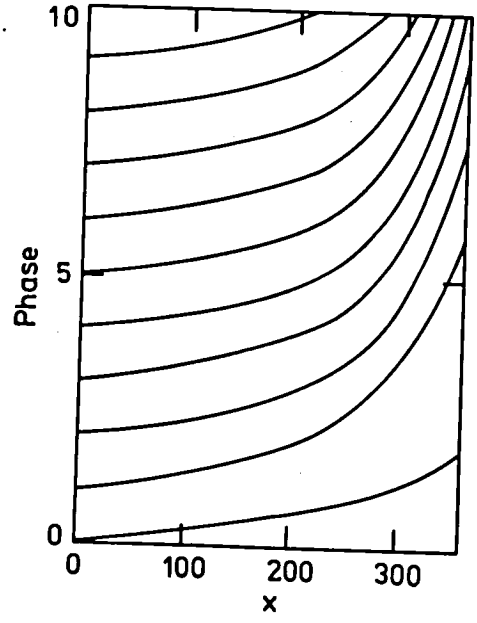

Fig. 4 Propagation of the first 10 shocks of the adiabatic calculations. x is the Eulerian coordinate (see § III).

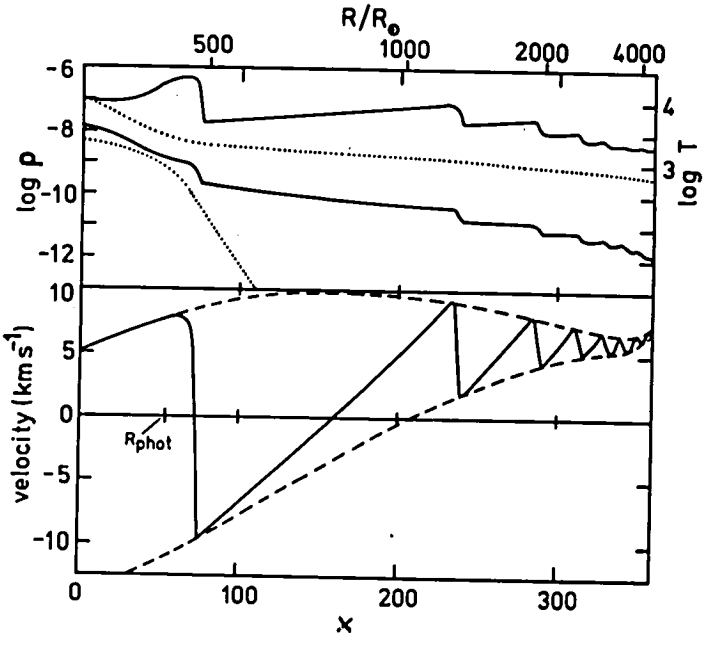

Fig. 5 Temperature, density and velocity profiles at a single phase of the adiabatic calculations after a steady state has been reached (continuous curves). Dotted lines show temperatures and density distributions in the initial hydrostatic models. Dashed lines mark an envelope for the velocity curves.

The rapidity of the first shock is due to two factors (a) the large density gradient in the hydrostatic atmosphere which causes the first shock to speed up (Zeldovich and Raiser 1966) more than later shocks when the density gradient has been reduced (see Fig. 5), and (b) the fact that all shocks but the first are impeded by the ram pressure of material falling inward after the passage of the previous shock. A further complication arises from the fact that in the steady periodic situation, the shocks are superimposed upon an underlying outward flow which causes the velocity amplitude of the shocks to decrease with time and radius even though they are propagating down a density gradient. These considerations show that the first shock is atypical and that therefore studies of the propagation of an individual shock into a hydrostatic atmosphere (e.g., Slutz 1975) do not give an accurate picture of the propagation of large-amplitude periodic shocks.

In the steady state, the shock waves are dissipated in the region above the photosphere and produce a steady mass outflow far from the star. Since the flow becomes supersonic before it reaches the outer boundary, the outer boundary conditions can not affect the flow, which must meet the interstellar medium in a shock front beyond the region studied here. Near the outer boundary, the velocity increases rapidly due to the formation of molecular hydrogen. The rate of continuous mass loss produced by the adiabatic pulsations is $\sim 0.02\ M_{\odot}\,yr^{-1}$, which is much greater than observational estimates of $\sim 2 \times 10^{-6}\ M_{\odot}\,yr^{-1}$ (Gehrz and Woolf 1971). However, the velocity of the outflow is similar to the observed values given in Figure 2.

The reason for the large mass loss rate is the high gas density in the flow. For a perfect gas, it is easy to show that the differential equations governing the continuous parts of the flow, and also the Hugoniot equations relating quantities across shocks embedded in the flow, are unaffected by a change of scale in the density. (Due to dissociation of hydrogen, the gas in the flow is not perfect at all points but the present arguments should remain essentially correct.) Thus the density at any point in the flow is proportional to the density or pressure specified at the inner boundary, while the flow velocity and temperature will remain unaltered following a change in scale of the inner boundary density or pressure. These considerations show that the mass loss rate could be lowered to observed values by reducing the inner boundary pressure by a factor of $\sim 10^4$. However, the resulting photospheric pressure and density are then considerably less than the observed values given earlier.

Another severe problem with these adiabatic models is the large region of high gas temperature ($T > 10^4$k) produced by pulsation. Assuming the high temperature post-shock region is optically thin to Balmer and higher series radiation, the cooling time at the densities involved for $T > 10^4$K is < 1 second. The adiabatic assumption is clearly violated in this situation. In view of the above considerations, it appears that adiabatic calculations do not accurately represent the behaviour of pulsation in the outer layers of Mira variables.

V. ISOTHERMAL MODELS

In these calculations, the temperature is time-invariant and has the radial distribution given by equation 1. A long series of models was computed covering 92 pulsation periods with a pressure variation amplitude

A = 1.0 (equation 2) at the inner boundary. Although no continuous mass loss was produced, occasional ejection of shells of material does occur.

The essential features of the dynamics of the situation can be explained with reference to Figure 6, in which the radii of the first 14 shocks are plotted against time. As in the adiabatic case, the first shock propagates rapidly outward down the density gradient in the hydrostatic atmosphere. Material behind the shock is decelerated by gravity and begins to fall in toward the star. The second shock begins to travel outward into the infalling material but is eventually halted and pushed backward. Each shock propagating outward reduces the amount of infalling material and the fourth shock actually overtakes and coalesces with shocks 2 and 3. This type of behaviour continues until after 14 cycles the inner regions (out to $\sim 600R_{\odot}$) become reasonably periodic. Typical velocity and density profiles after many cycles are shown in Figure 7. In the extended calculations, the continual coalescing of shocks beyond the periodic region eventually (after 80 cycles) built up a single strong shock which was able to propagate outward and escape through the outer boundary. By repeated events of this type, a Mira variable could build up a circumstellar shell and possibly produce a mass outflow. However, the mass loss rate (calculated by dividing the mass lost in the single ejection event by the time required to produce this event) is very small ($\sim 10^{-12} M_{\odot} yr^{-1}$).

The variation of post shock velocity with phase is shown in Figure 8. It is interesting that the rise to maximum at phase 0.1 - 0.2 and subsequent decline is similar to the results obtained from the early observations shown in Figure 3a. The maximum value of the theoretical post-shock velocity lies well within the range of emission line velocities exhibited by the sample of stars in Figure 1.

A recent observation (Hinkle 1978) which can be compared with the present isothermal calculations is the infra-red absorption line radial velocity curve of R Leo (Fig. 9), which indicates infall velocities much greater than those previously obtained from optical observations (Fig. 1). Although the precise point of origin of the IR absorption lines in the dynamical atmosphere is not known, the maximum infall velocity in the atmosphere at any time must be at least as large as that obtained from the IR observations. It can be seen from Figure 9 that the infall velocity at the nominal photosphere ($\tau = \frac{2}{3}$) of the isothermal models accelerates at almost the same rate as the infall velocity observed in R Leo, except for the flat spot on the velocity curve of the models (caused by the hydrogen dissociation region moving close to the photosphere as the pressure falls). This indicates that the surface gravity g (or more precisely, g times the pulsation period P) of R Leo is approximately the same as that of the present models but that the temperature in the models should be raised slightly to prevent formation of molecular hydrogen in the photospheric region. This latter suggestion is also consistent with the fact that Hinkle (1978) derives temperatures > 3000K for the regions in which the lines used to derive the velocities in Figure 9 are formed. Although R Leo has a shorter period (312 days) than the models (373 days), the formulae of Wood and Cahn (1977) predict an effective temperature for R Leo which is only 50K hotter than that in the models and a value of gP only 6% greater.

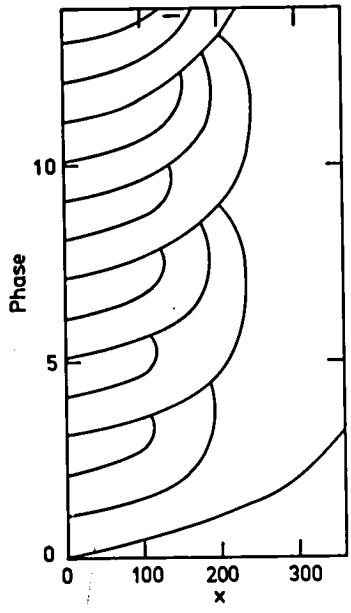

Fig. 6 Propagation of the first 14 shocks of the isothermal calculations.

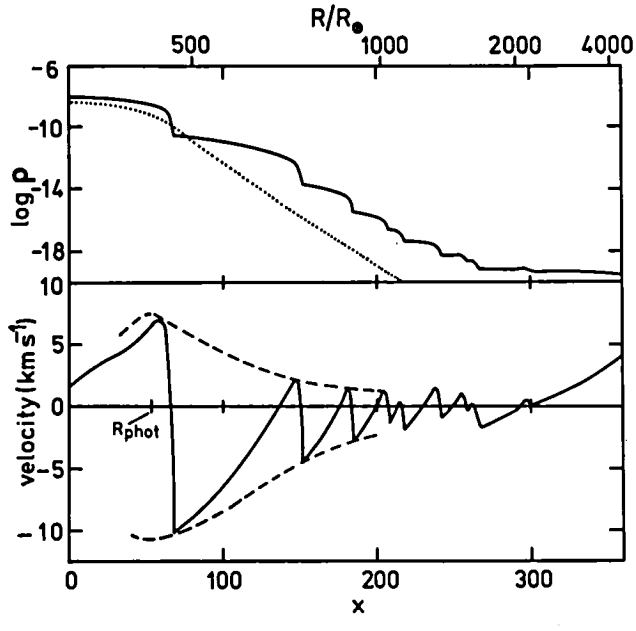

Fig. 7 Density and velocity profiles at a single phase of the isothermal calculations (continuous curves). The dotted line shows the density distribution in the hydrostatic starting model. The upper dashed curve is drawn through the post-shock velocity maxima and the lower dashed curve indicates maximum infall velocity. The positive velocity at the outer boundary was caused by passage of a shock (see text).

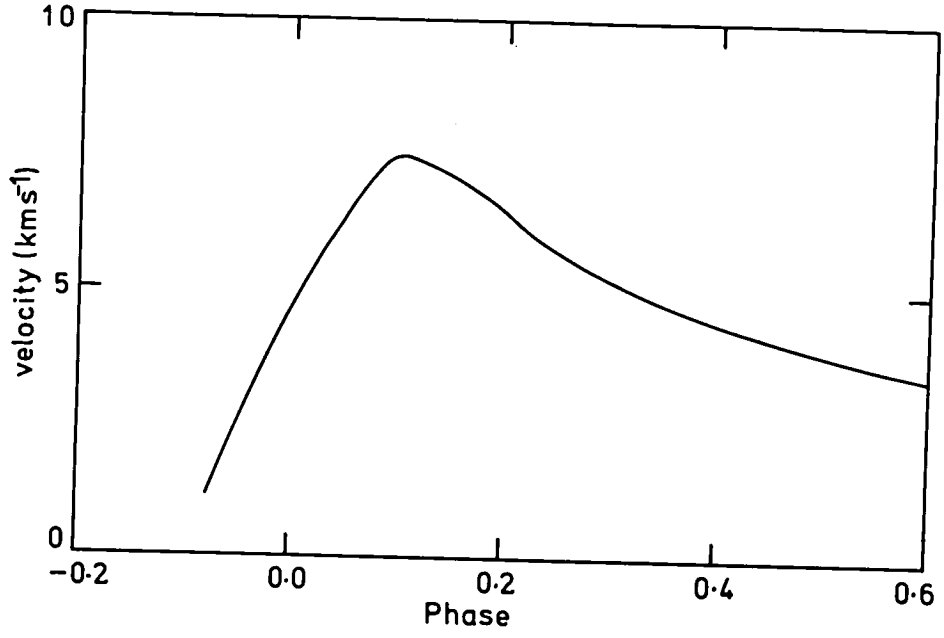

Fig. 8 Post-shock velocity plotted as a function of phase in the isothermal models. The zero point of phase is shifted so that the velocity maximum occurs near the phase of the observed velocity maximum in Figure 3a.

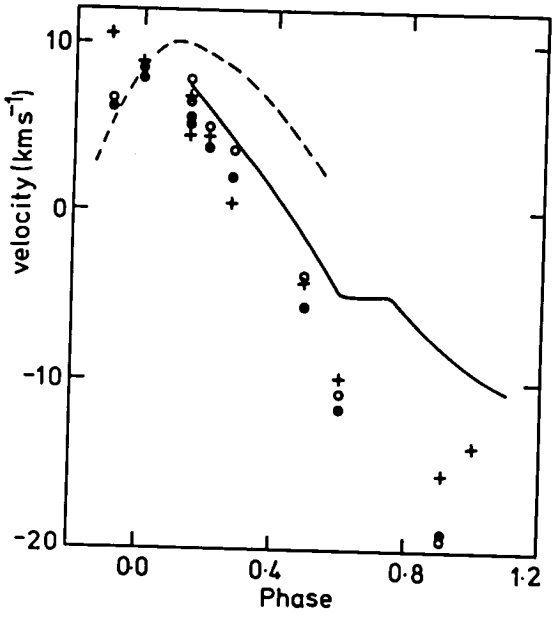

Fig. 9 The velocity at the nominal photosphere ($\tau = \frac{2}{3}$) of the isothermal models plotted against phase (continuous curve). The symbols are infra-red absorption line velocities of R Leo (relative to the centre-of-mass given in Table 1) from Hinkle (1978): ,CO Δv = 3 lines; +,CO Δv = 2 high excitation lines; O,OH Δv = 2 lines. The dashed curve is the hydrogen emission line velocity of R Leo from Figure 3a.

VI. THE EFFECT OF PULSATION ON A MASS FLOW PRODUCED BY RADIATION PRESSURE

Using the approximations given in § III for grain formation and acceleration by stellar radiation, the effective grain radiation cross-section parameter Q_{eff} was adjusted (keeping the inner boundary pressure constant) until a steady outward flow was obtained with a velocity at the outer boundary of ~ 5 km s^{-1} (Fig. 10). Integrating the flow from the

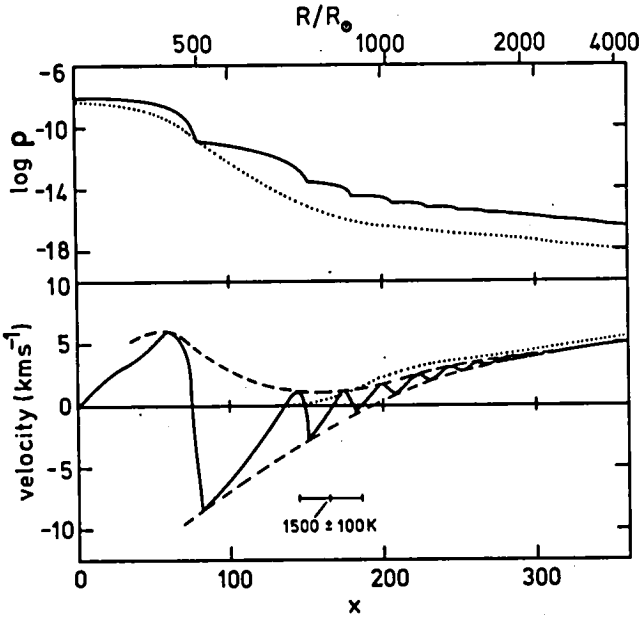

Fig. 10 Density and velocity profiles at a single phase in the models which include a radiation pressure-induced mass flow as well as pulsation. Dotted lines show density and velocity profiles in the initial steady state mass outflow model. The dashed curves are an envelope to the velocity profiles.

outer boundary to infinity gives a terminal velocity of 7 km s^{-1}, which is well within the range of observed flow velocities (Fig. 2). The mass loss rate Φ resulting from the flow is 7×10^{-9} $M_\odot yr^{-1}$. However, this value is not very meaningful since Φ is directly proportional to the pressure Π specified at the inner boundary (see § IV.). Any value of Φ can be obtained by adjusting Π, while the flow velocity will remain unaltered.

The effect of a pulsating atmosphere (isothermal approximation) at the base of the steady mass outflow was examined by varying the pressure at the inner boundary (using an amplitude A = 1.0 in equation 2) so that pulsation and shock waves were produced as before. Figure 10 shows the initial density and velocity distributions and the distributions which resulted when an equilibrium situation had been attained. The two main results of this calculation are (1) the flow velocity far from the star is only slightly different from that which existed in the absence of pulsation, and (2) the mass loss rate is increased by a factor of ~ 40. The latter result is due

to the lowering of the time-averaged density (or pressure) scale height in the pulsating regions below the sonic point causing the sonic point density to be raised.

As a final point, it is noted that in the region where pulsation velocities are much greater than the underlying flow velocity (radius $< 600R_\odot$), the behaviour of pulsation is almost identical to that which occurs when there is no radiation pressure-induced mass loss (the maximum post-shock velocity is slightly smaller in these calculations but this is purely a result of the increased numerical smoothing of the velocity profile behind the shock caused by the doubling of the zone spacing used in the isothermal models without grains). Since the emission lines in the model come from shocks at radii $< 600R_\odot$, no information relating to the mass outflow can be obtained from shock emission.

VII. SUMMARY

It has been shown that adiabatic pulsation in the surface layers of a star with parameters similar to those of a Mira variable can produce a steady stellar wind with a terminal velocity similar to that observed in the stellar winds associated with Mira variables and cool luminous red giants. However, two direct consequences of the adiabatic models conflict with observations (1) with observational estimates of the photospheric density, the mass loss rate is $\sim 10^4$ times larger than observed, and (2) an extensive region with a temperature $> 10^4$K exists behind the innermost shock and since the cooling time for this region is much shorter than the pulsation period, the assumption of complete adiabaticity is clearly incorrect.

Mira-type pulsation in the envelope of a red giant is found incapable of producing a continuous mass outflow when the radial temperature distribution is held constant in time (isothermal approximation). However, the coalescing of many shock waves in the outer layers of the envelope causes occasional ejection of shells of matter. The mass loss rate estimated for this process is $\sim 10^{-12} M_\odot yr^{-1}$. Since this mass loss rate is much smaller than observed mass loss rates, another mass loss mechanism, such as the action of radiation pressure on grains, must exist on the giant branch. The magnitude of the post-shock velocity in the isothermal models is shown to agree reasonably well with the velocity of the hydrogen emission lines observed in Mira variables.

In order to investigate the effect of pulsation on a stellar wind produced by the action of radiation pressure on grains, a model was first produced with a steady radiation pressure-induced mass outflow and then pulsation was introduced into the star. The flow velocity far from the star was almost unaltered by the pulsation but the mass loss rate was enhanced by a factor of ~ 40. Thus Mira variables can be expected to lose mass at a rate which is considerably faster than that in non-variable red giants of similar luminosity and spectral type. The enhancement in the mass loss rate is due to the reduced density gradient in the pulsating atmosphere and the consequent increase in the density at the sonic point of the flow.

This work was performed while the author was in receipt of a Queen Elizabeth II Fellowship at the Australian National University.

References

Auman, J. R.: 1969, Ap.J. 157, 799.
Bernat, A. P.: 1977, Ap.J. 213, 756.
Bowers, P. F. and Kerr, F. J.: 1977, Astr. and Ap. 57, 115.
Caswell, J. L., Robinson, B. J. and Dickel, H. R.: 1971, Astrophys. Letters 9, 61.
Deutsch, A. J.: 1960, in Stellar Atmospheres (Chicago: University of Chicago Press), ed. J. L. Greenstein, P.543.
Dickinson, D. F. and Kleinmann, S. G.: 1977, Ap.J.(Letters). 214, L135.
Dickinson, D. F., Kollberg, E. and Yngvesson, S.: 1975, Ap.J. 199, 131.
Dickinson, D. F., Reid, M. J., Morris, M. and Redman, R.: 1978, Ap.J. 220, L113.
Elitzur, M., Goldreich, P. and Scoville, N.: 1976, Ap.J. 205, 384.
Feast, M. W.: 1963, M.N.R.A.S. 125, 367.
Fujita, Y.: 1970, Interpretation of Spectra and Atmospheric Structure in Cool Stars (Tokyo: University of Tokyo Press), p. 89.
Fussi-Pecci, F. and Renzini, A.: 1976, Astr. and Ap. 39, 413.
Gehrz, R. D. and Woolf, N. J.: 1971, Ap.J. 165, 285.
Harvey, P. M., Bechis, K. P., Wilson, W. J. and Ball, J. A.: 1974, Ap.J. Suppl. 27, 331.
Hinkle, K. H.: 1978, Ap.J. 220, 210.
Hoyle, F. and Wickramasinghe, M. C.: 1962, M.N.R.A.S. 124, 417.
Joy, A. H.: 1926, Ap.J. 63, 281.
1954, Ap.J.Suppl. 1, 39.
Kwok, S. 1975, Ap.J. 198, 583.
Lo, K. Y. and Beckis, K. P.: 1977, Ap.J. (Letters), 218, L27.
Maciel, W. J.: 1977, Astr. and Ap. 57, 273.
McGee, R. X., Newton, L. M. and Brooks, J. W.: 1977, M.N.R.A.S. 180, 91p.
Merrill, P. W.: 1945, Ap.J. 103, 6.
————————: 1945a, Ap.J. 103, 275.
————————: 1947, Ap.J. 106, 274.
————————: 1952, Ap.J. 116, 337.
————————: 1953, Ap.J. 118, 453.
Merrill, P. W. and Burwell, C. G.: 1930, Ap.J. 71, 285.
Nguyen-Quang-Rieu, Fillet, R. and Gheudin, M.: 1971, Astr. and Ap. 14, 154.
Reid, M. J. and Dickinson, D. F.: 1976, Ap.J. 209, 505.
Reid, M. J., Muhleman, D. O., Moran, J. M., Johnston, K. J. and Schwartz, P.R.: 1977, Ap.J. 214, 60.
Reimers, D.: 1977, Astr. and Ap. 61, 217.
Renzini, A., Cacciari, C., Ulmschneider, and Schmitz, F.: 1977, Astr. and Ap. 61, 39.
Sanner, F.: 1976, Ap.J.Suppl. 32, 115.
Slutz, S.: 1976, Ap.J. 210, 750.
Wallerstein, G.: 1975, Ap.J.Suppl. 29, 375.
Weyman, R. J.: 1962, Ap.J. 136, 476.
————————: 1963, Ann. Prev. Astr. and Ap. 1, 97.
Wilson, W. J. and Barrett, A. H.: 1972, Astr. and Ap. 17, 385.
Wilson, W. J., Schwartz, P. R., Neugebauer, G., Harvey, P. M., and Becklin, E. E.: 1972, Ap.J. 177, 523.
Wood, P. R.: 1975, M.N.R.A.S. 171, 15p.
Wood, P. R. and Cahn, J. H.: 1977, Ap.J. 211, 499.
Zel'dovich, Ya. B. and Raizer, Ya. P.: 1966, Physics of Shock Waves and High-Temperature Phenomena (London: Academic Press).

Discussion

J. Wood: In one of your earlier slides, where you showed the series of shocks asymptotically approaching 7 km/sec, at what point does the escape velocity fall to this value?

P. Wood: At about 2000 solar radii, or a bit beyond. It has become supersonic at that point.

J. Cox: I don't understand why you had to assume it is isothermal. When you do the calculation, the energy equation...

P. Wood: Either you have to know all the physics of the shock -- that is, how much energy is being radiated in lines behind the shock, etc. -- or you can do the simple thing by assuming it's adiabatic (and then you use the energy equation), or you can assume it's isothermal (in which case, you assume that in a region which is very thin relative to the separation of the two shocks, all the energy is radiated). Those are the two limits I took, adiabatic and isothermal, without doing all the detailed physics.

Willson: We also did the same calculation and found the same results, that the isothermal model does not show mass loss. 10^{-12} is the number that we estimated in the same fashion as you did. I am very pleased to see that you calculated the combination of dust with the isothermal case, and I was as startled as anyone else to find that it only gives you a factor of 40, which is not enough to give you the six orders of magnitude that you need. Although we have not yet run the right masses, we found that if you look carefully at what's happening in the shock, the isothermal model should break down at

several stellar radii, because the recombination length of hydrogen in the shock becomes comparable to other scales of the problem. At that point, you start to convert to the adiabatic approximation. At that point you lose a lot of mass. If you estimate where that point occurs and calculate the mass loss, it is within a factor of 10 of 10^{-6}. As I said, we haven't run the exact models, but that looks like the right ball-park estimate; that's closer than anything else that's been done.

P. Wood: By the time you get into those regions, the shock is so "thick" that it's meaningless to talk about a shock wave.

Unknown: Barkat would argue with you that you can't do it with pulsation. He said that you could do it by a series of puffs blown off by individual pulsations which sort of build up, pop, and then settle down.

P. Wood: Yes, these are relaxation oscillations, which are of much larger amplitude. They don't bear any resemblance to what you see in a Mira. That is something later in the evolution.

Keller: Are you aware of Sanford's IR image tube observations, which show a very extended dust cloud around α Ori? He just recently published these 1 μ observations. In other unpublished work, he has seen a large cloud around R Leo, which would extend out to enormous distances, as you might expect.

Van Horn: To more than 100 stellar radii?

Keller: Oh, yes.

P. Wood: R Leo has a larger IR excess than most Miras of the same type.

Nather: There are occulation measurements of R Leo in the IR at Hale Observatory, that are 10-100 times larger than what we see in the optical region. That would tend to bear this out.